F.S.A.I. Vol. 10, No. 3, pp. 36-55, 2004

Hysteretic Fuzzy Control of the Power Interface Converter

N. Bizon(*), M. Oproiescu(*)

* University of Pitesti, Pitesti

Abstract: A hysteretic controller represents a suitable control solution for a process with a linear /nonlinear static characteristic of transfer. In this paper a boost converter it was chosen to be an interface of the power conversion in a typical energy generation system with an energy storage device (ESD) used as a load energy buffer. The Boundary Control with Current Taper (BCCT) transfer characteristic solves the ESD interfacing problems for nominal or near to nominal load conditions. If the power conversion process is parametrically disturbed in time or the load has a large dynamic the control performances of the BCCT controller are spoiled. In this work it's proposed a control structure (named Hysteretic Fuzzy Controller - HFC) that consists in a Basic Hysteretic Controller (BHC) which practically controls the switching process and a fuzzy controller. The boundary control law adaptation is done on-line based on fuzzy linguistic rules, depending on: the evolution of the output voltage and inductor current ripple. The inductor current ripple and the power conversion efficiency are depending by the switching frequency, so the clocked controller variants (CBCH, CBCCT and CHFC) are analyzed, too. The obtained results are very promising, validating the model of the proposed control. The converter efficiency using the (C)HFC isn't presented in this paper. Ideal switching models are used for electronic devices. In this paper we present some significant simulation results that are obtained when the switching controller is (C)BHC, (C)HFC or (C)BCCT), respectively, for a large dynamic load.

1 Introduction

1.1 Boost Converter Structure

The boost converter topology used [1,2,3] is shown in figure 1 without (a) and with ESD like load energy buffer (b).

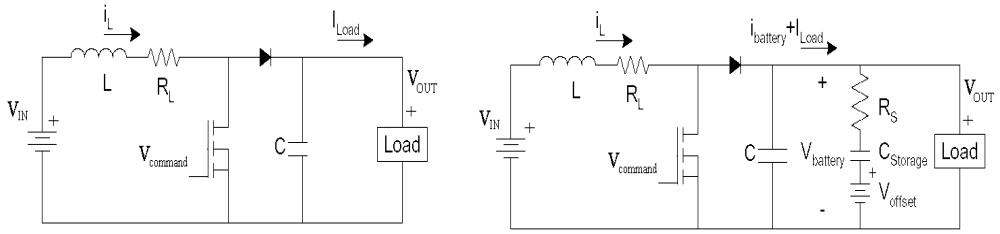

a) without ESD b) with ESD

Fig. 1 - Boost converter topology

For the initial converter designing we ignore the series resistance R_L of the inductor L (but we use RL = 0,05Ω in all simulations) and we consider that the

output load is constant (at a nominal value), so the switching frequency $f = \frac{1}{T}$ is constant, too (10 kH for nominal conditions or the clock value for clocked controller).

The boost converter equation, when this operates in continuous conduction mode (CCM), is $\frac{V_{out}}{V_{in}} = 1 - \tau$, where $\tau = \frac{t_{on}}{T}$ is the duty ratio. In this paper the nominal conditions for the input voltage, output voltage and output power are $V_{in} = 48V$, $V_{out} = 60V$ and $P_{out} = 900W$, respectively. Result $I_{load} = 15A$ and $R_{load} = 4\Omega$. If the work switching frequency is 10 kHz (approx. or fixed) and the duty ratio is $\tau = 0{,}2$, the average inductor current (<iL>= IL) is $I_L = \frac{I_{out}}{1-\tau} = 18{,}75A$. The inductor current ripple is a function of the switching frequency, duty ratio, inductance value and current control mode.

We choose the current control mode for boost converter operation to limit the inductor current ripple (necessary for most energy sources). In many cases, especially in the energy storage technologies, the boost converter works like a power interface between a (renewable) energy source and an energy storage device [4,5]. Figure 2 shows a block diagram of a typical energy generation system with an energy storage device used as the energy buffer.

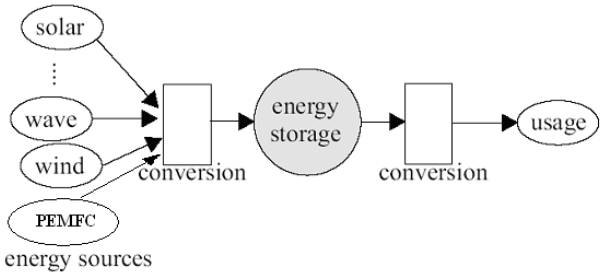

Fig. 2. A typical energy generation system with energy storage

Using the graphical representation of the specific energy [Wh/kg] versus specific power [W/kg] for various energy storage technologies from the literature [6], we conclude that the highest specific energy is achieved by the electrochemical technologies, but at the lowest specific power, and the highest specific power is reached by the electrical field technologies, but at the lowest specific energy.

1.2 Boost Converter Model without ESD

In the current control mode, when a light load produces a low average inductor current, the converter operates in discontinues conduction mode (DCM). So, there are three possible states or circuit configurations that depend by the state (q1) of

the electronic switch (controlled by command voltage $v_{command}$) and the diode conduction state (q2). [7,8]. Each one of these configurations can be expressed as a second order differential system of equations. Then, weighting the contribution of each switching configuration, a complete expression can be written for each of the state variables:

$$\frac{di_L}{dt} = q_1 \frac{V_{in} - I_L \cdot R_L}{L} + q_2 \frac{V_{in} - I_L \cdot R_L - v_{out}}{L} \quad (1)$$

$$\frac{dv_{out}}{dt} = q_1 \frac{-v_{out}}{R_{load} \cdot C} + q_2 \frac{i_L - v_{out} / R_{load}}{C} \quad (2)$$

where v_{out} is the output voltage and i_L is the inductor current. In fact this is a well know average model [9,10] of the boost converter shown in figure 1.a. The electronics devices are modeling by ideal switches.

1.3 Boost Converter Model with ESD

In this paper, we choose a lead-acid battery for the energy storage device (ESD). Generally, a battery model is complex because the storage device has many model parameters such as capacity, dead-cell voltage, discharge impedance, self-discharge impedance, and shunt capacitance. In order to simplify the simulations is used (from specialized literature [11]) a simple model for a sealed lead acid (SLA) battery.

The battery is modeled as a capacitor for energy storage $C_{storage}$, a DC offset voltage V_{offset} and a series resistance R_s to limit the short circuit current (figure 1.b). In this paper, the 60V/7Ah battery pack has the structure: 5 batteries, 6 cells/battery and 2,45V max/cell. The value of series resistance is taken as 80mΩ/cell (as suggested in [11]).

The calculated equivalent series resistance of the pack is RS=5·80 mΩ=0,4 Ω. The typical "dead cell" voltage for SLA technology is about 1,75V. Therefore the total offset voltage is V_{offset}=5·6·1,75 V=52,5 V. Lastly, the energy stored in the capacitor can be calculated. First we calculate the maximum battery pack voltage: V_{max}=5·6·2,45 V=73,5 V. So, the maximum storage capacitor voltage must be the difference between the maximum expected battery voltage and the dead-cell voltage: $V_{C\_storage} = V_{max} - V_{offset}$ =21 V. For the 7Ah batteries we obtain Q=7 Ah·3600sec/hour=25200 C and the value for the modeled storage capacitance is $C_{storage} = Q / V_{C\_storage}$ =1200 F.

The average model of the boost converter interface shown in figure 3 is described by three differential equations that expands the system to a third order system (three state variable: v_{out} , i_L and voltage over the $C_{storage}$ - $v_{C\_storage}$):

$$\frac{di_L}{dt} = q_1 \frac{V_{in} - i_L \cdot R_L}{L} + q_2 \frac{V_{in} - i_L \cdot R_L - v_{out}}{L}$$
$$\Rightarrow \frac{di_L}{dt} = \frac{V_{in} - i_L \cdot R_L - q_2 \cdot v_{out}}{L} \quad (3)$$

$$\frac{dv_{out}}{dt} = q_1 \frac{-(i_{battery} + I_{load})}{C} + q_2 \frac{V_{in} - i_L \cdot R_L - v_{out}}{C}$$
$$\Rightarrow \frac{dv_{out}}{dt} = \frac{-(i_{battery} + I_{load}) + q_2 \cdot i_L}{C} \quad (4)$$

$$\frac{dv_{C\_storage}}{dt} = q_1 \frac{v_{out} - v_{C\_storage} - V_{offset}}{C_{storage}} \quad (5)$$

Obviously, the addition of the battery to the boost converter output change the control characteristic that must consider the required battery charging parameters in the control law generation.

2 Hysteretic Controller

2.1 Basic Hysteretic Control

Hysteretic current-mode control, which the Bose Corp patented in 1984 [12], has remained an obscure technique for many designers, yet it offers significant advantages for many applications. Hysteretic current-mode control (HCMC) offers the tightest and most accurate control of the inductor current, is unconditionally stable regardless to duty cycle, and offers excellent transient response to step loads.

The general concept in the hysteretic control is to place the control law such that the phase space of the variables (v_{out} and i_L) is divided into two regions with the "on" and "off" equilibrium points residing in different regions in the phase space [13]. Because the system evolves and the state variables approach an equilibrium point, the trajectory crosses the graphical boundary and initiates a switch action. The new system begins to evolve and the trajectory moves toward the new equilibrium point that depend by the initial and steady state condition ($V_{out}(0)$, V_{in}, V_{out} and P_{out}).

The first set of the simulation examples use pure boundary control (BHC) laws. The switch action is based solely on the state variables. The advantage of such a system is that the control is relatively simple to implement and the switch actions are done at request. If the load suddenly is dropped, the switching interval or period correspondingly increases. The hysteretic controller illustrates how switch action is initiated based on the value of the inductor current. For an inductor current less than $I_{L\min} = I_L - \Delta I_L / 2$ the boost switch is turned on, causing the inductor current to ramp up. The capacitor voltage drops as the capacitor discharges to support the

load current. When the inductor current reaches $I_{L\max} = I_L + \Delta I_L / 2$ the boost switch is turned off, the wheeling diode (forward biases) is turning on. The capacitor voltage raises as the inductor current supports the load and the capacitor recharges. The BHC law can be expressed analytically as:

$$I_{\lim(\max)(\min)} = I_{L(\max)(\min)}, \quad 0 < V_{out} \le V_{\max} \tag{6}$$

The first of the following simulations assume zero energy storage as initial conditions $v_{out}(0)=0$, the mention steady state conditions and choosing supplementary the steady state conditions: inductor current ripple $\Delta I_L < 2\,\text{A}$ and output voltage ripple $\Delta V_{out} < 2$. These two last parameters allow the boost converter energy storage components and the hysteretic current control circuit design:

$$V_{in} = L\frac{di_L}{dt} \Rightarrow L = \frac{V_{in}\cdot t_{on}}{\Delta I_L} \tag{7}$$

$$I_{load} = C\frac{dv_C}{dt} \Rightarrow C = \frac{I_{load}\cdot t_{on}}{\Delta V_{out}} \tag{8}$$

We can use HCMC with most switching-regulator topologies, including buck, forward-mode, boost, and continuous-mode flyback converters. HCMC ideally suits applications that require control of both load current and output voltage. Also these applications require that power supplies behave as constant-current sources and as constant-voltage regulators. Examples of these applications include battery chargers, arc welders, fluorescent lamps, laser power supplies, and servo-motor control circuits.

2.2 Hysteretic Control with current taper transfer characteristic

Like we said, for the boost converter that interface the energy source and the ESD in parallel with load (figure 1.b), we must consider the battery charging requirements in the control law. The solid line in figure 3 represents the new boundary control law (named *boundary control with current taper-BCCT).* This is a function of both current limits and battery voltage [14]. Regardless to the commanded current, as the batteries charge and the voltage increases (over knee voltage V_{knee}, to the maximum value V_{mas}), the inductor peak current will back off to prevent “boiling” of the batteries.

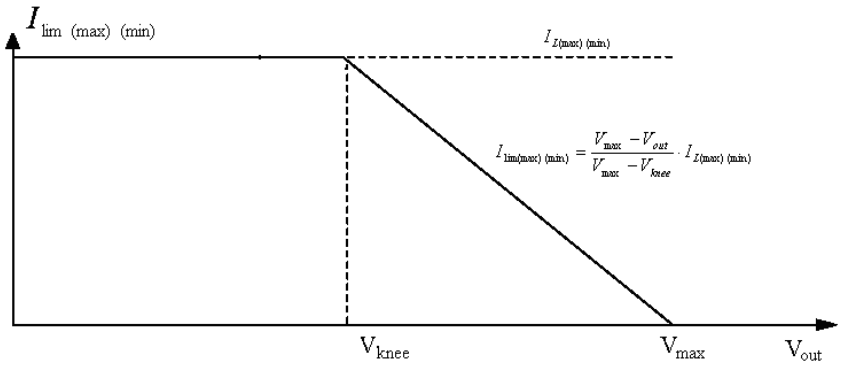

Fig. 3 BCCT current limit control law

The BCCT law can be expressed analytically as:

$$I_{\lim(\max)\,(\min)} = \begin{cases} I_{L(\max)\,(\min)}, & 0 < V_{out} < V_{knee} \\ \dfrac{V_{\max} - V_{out}}{V_{\max} - V_{knee}} \cdot I_{L(\max)\,(\min)}, & V_{\max} \geq V_{out} \geq V_{knee} \end{cases} \tag{9}$$

A control structure that can implements both (BCH and BCCT) control laws is shown in figure 4.a. Boundary Control Law Generation (BCLG) block gives the limits for inductor current when BHC it is used. For the BCCT implementation BCLG block makes the correction of the BHC law, according to the BCCT law when the output voltage bigger than knee voltage, V_{knee}:

$V_{knee} = 5 \cdot 6 \cdot 2.13V \cong 64\,\mathrm{V}.$

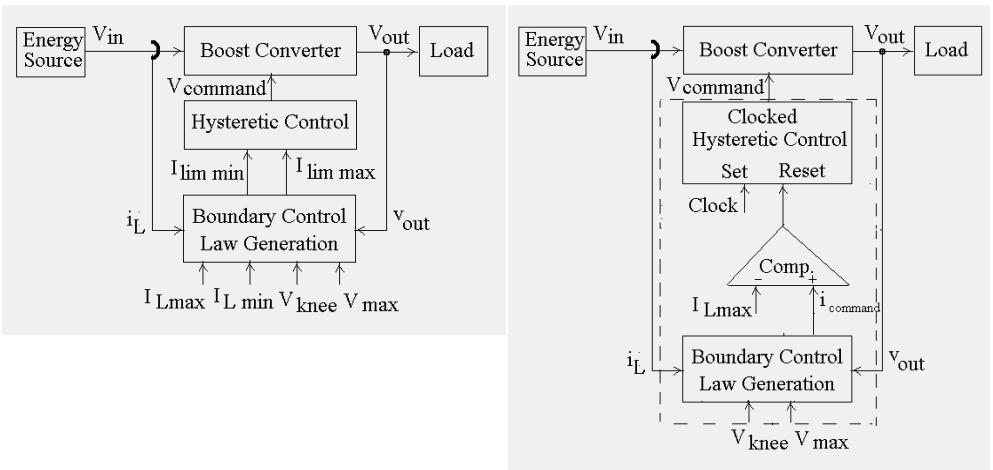

a) without clock b) with clock

Fig. 4 - Hysteretic Controller

Finally, the control circuit is more complex (see figure 4.b) and isn't very robust to load perturbation A disadvantage in this scheme is that there is no enforced switching frequency. The operating mode of the converter is based completely on the values of the energy storage components (boost inductor and output capacitor) and current limits (I_{lim_max} and I_{lim_min}). If the values are small enough, the converter operates in "sliding mode" [15], where the switching frequency is fast and the state variables have small deviations about the boundary control law. If the values of the inductor and capacitor are large, the circuit operates at a lower frequency and the state variables generally have larger ripple components.

Today, some nice features of hysteretic controllers make this mode of operation so popular that large semiconductor manufacturers introduced a hysteretic mode converter last decade. Since the first current-mode control ICs emerged in the early 1980s, the popularity of current-mode control has made it the method of choice for most power supplies. Although there are a number of different types of current-mode control [16], the most popular is constant frequency with turn on at clock time.

Constant-frequency control has become synonymous with current-mode control for most designers. Comparing the operation of constant-frequency and hysteretic-mode controllers highlights major differences. Figure 6 shows a simplified block diagram of a constant-frequency current-mode regulator. The clock or oscillator sets the RS flip-flop each cycle and turns on power-switch Q1 while the control loop determines the period for which it remains on. The external RT/CT network determines the operating frequency.

In figure 6, the controller detects the peak inductor current by sampling the voltage across RS while sampling the output voltage VOUT directly. Depending on the value of VOUT, the output of the error amplifier determines the peak current that flows in the inductor by constantly adjusting the voltage level on the inverting terminal of the current-sense comparator. The controller detects any change in the input voltage by detecting a change in the peak current measured as a voltage across RS; it then adjusts the on-time of the FET to hold VOUT constant.

Figure 5.a shows a similar regulator that uses a hysteretic-mode control system. In HCMC, no oscillator exists. The regulator senses inductor current by monitoring the voltage across RS using a differential current-sense amplifier. This amplifier's output drives two comparators, IL max and IL min. The inductor current iL ramps alternately between an upper limit $I_{L\ max}$ and a lower limit $I_{L\ min}$ (figure 5.b).

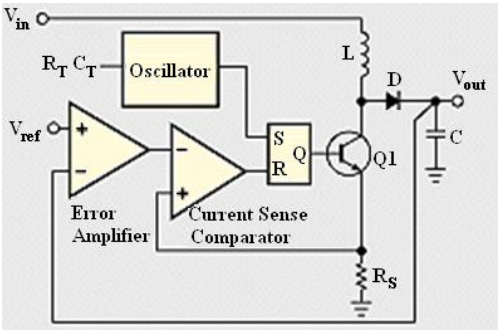

Fig 5 - An external R/C network determines the fixed operating frequency of a constant-frequency

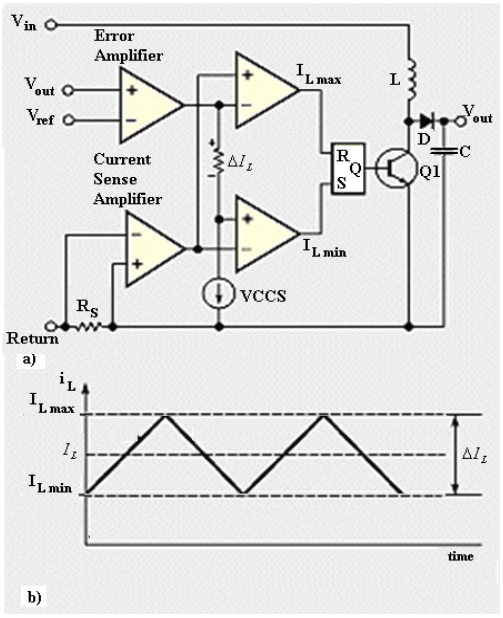

Fig 6 - A hysteretic-mode controller (a) maintains a difference (ΔI_L) between two comparators, and inductor current increases and decreases between the comparators' $I_{L\,max}$ *and* $I_{L\,min}$ *thresholds (b).*

2.3 Clocked Hysteretic Control

In a clocked hysteretic model (figure 4.b) a set-reset flip-flop is used to toggle the main switch (a MOS transistor, in general). The master clock sets the flip-flop while the current limit resets the flip-flop. The duty ratio of the clock is set to low value (in all presented simulations is 1% or equivalent 1μs time on; sufficient time for turn on the MOS transistor at 10 kHz switching frequency). This small value it was chosen to prevent the clock interference with the action of the current limit reset (IL_max), when this limit is compared with command current - $i_{command}$. A reset dominant SR latch action is desirable.

The CBHC command current law can be expressed analytically as:

$$i_{command} = i_L \tag{10}$$

and the CBCCT command current law can be expressed analytically as (figure 7):

$$i_{command} = \begin{cases} i_L, & 0 < V_{out} < V_{knee} \\ \dfrac{V_{\max} - V_{out}}{V_{\max} - V_{knee}} \cdot i_L, & V_{\max} \geq V_{out} \geq V_{knee} \end{cases} \tag{11}$$

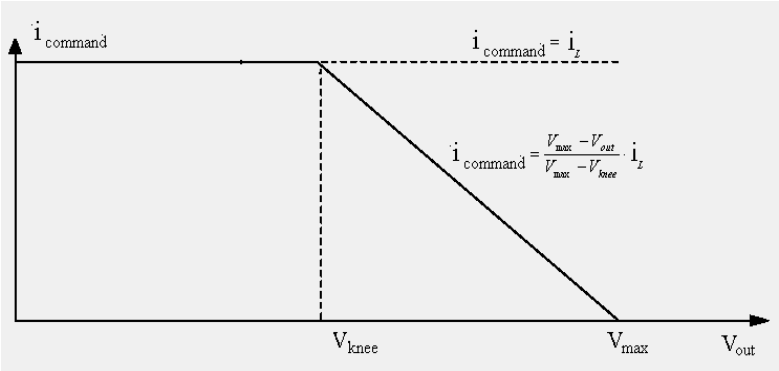

Fig. 7. CBHC and CBCCT control laws

By controlling the turn on of the switch, the frequency of the switching action is controlled and the duty ratio is automatically determined by the current limit control. At the fixed 10 kHz switching frequency, inductor and capacitor size are now easy to calculate using the relations (7) and (8). A "reset dominant" flip-flop is desired to prevent the clock to turn on the MOS transistor if the inductor current is above the threshold – for example at startup or other transient conditions, the converter can operate in "pulse skipping" mode (see simulation results following shown). Obviously, for a dynamic load we can't find optimal values for L and C, so fuzzy control must be a solution for a stable and robust control.

3 Hysteretic Fuzzy Controller

The structure of the HFC (shown in figure 8) is following defined:

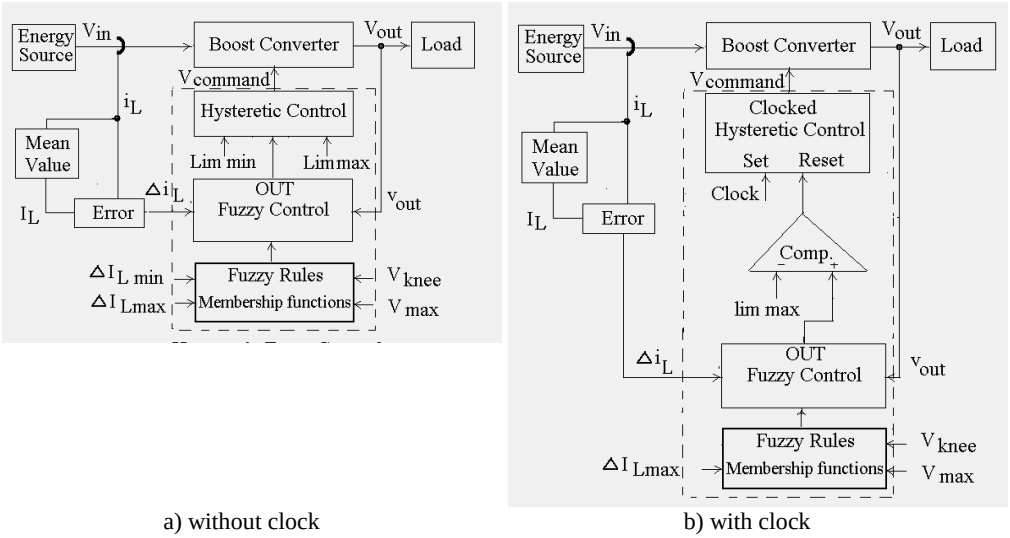

a) without clock b) with clock

Fig. 8 - Hysteretic Fuzzy Controller

- the inputs: $\Delta i_L = i_L - I_L$ (input 1) on [$-\Delta I_{LMM}$, ΔI_{LMM}] and v_{out} (input 2) on [0, V_{MM}], respectively, where $\Delta I_{LMM} > I_{L\max}$ $V_{MM} > V_{\max}$;

- the output: out on [0, m], $m \in \Re^*$ (for all presented simulation we choose m=100);

- trapezoidal membership functions for Δi_L (see table 1), where ΔI_{Lnom} fix the nominal inductor current ripple, with boundary limits $Lim_{\max}$ and $Lim_{\min}$, too. We choose $\Delta I_{Lnom} = \Delta I_{L\max}$ for HFC and $\Delta I_{Lnom} = \frac{\Delta I_{L\max} + \Delta I_{L\min}}{2}$ for CHFC and we control the inductor current ripple by boundary limits;

- trapezoidal membership functions for v_{out}. Membership functions for input fuzzy variables are defined correlate with output voltage parameters (V_{offset}, V_{kneet}, $V_{\max}$) and inductor current ripple (ΔI_{Lmax}, ΔI_{Lmin});

- trapezoidal membership functions for out;

- the rule list: (N, L, B), (ZE, L, M), (P, L, S), (N, N, M), (ZE, N, M), (P, N, S), (N, H, S), (ZE, H, S), (P, H, S);

- Zadeh fuzzy connectives (max-min) and Mamdani implication [17,18,19].

Fuzzy rules generate a control surface witch in output voltage section have the same shape allure with CBCCT control law.

Table 1

Membership functions for fuzzy variables

	Fuzzy variables		
	$\Delta i_L = i_L - I_L$	v_{out}	out
Membership functions	**N**egative (**N**)= ($-\Delta I_{LMM}$, $-\Delta I_{LMM}$, $-\Delta I_{Lnom}$, 0), **Z**ero Equal (**ZE**)= ($-\Delta I_{Lnom}$, 0, 0, ΔI_{Lnom}), **P**ositive (**P**)= (0, ΔI_{Lnom}, ΔI_{LMM}, ΔI_{LMM})	**L**ow (**L**)= (0, 0, V_{offset}, V_{knee}), **N**ormal (**N**)= (V_{offset}, V_{offset}, V_{knee}, V_{knee}), **H**igh (**H**)= (V_{knee}, V_{max}, V_{MM}, V_{MM})	**S**mall (**S**)= (0, 0, m/4, m/2), **M**edium (**M**)= (m/4, m/2, m/2, 3m/4), **B**ig (**B**)= (m/2, 3m/4, m, m)

4 Simulation results

For all presented (C)HFC simulation we choose ΔI_{LMM}=40 A, $V_{MM} = 80$ V and m=100. Obviously, the ΔI_{Lnom} membership function parameter can be used to adjust the nominal inductor current ripple, but utilization of the boundary limit $Lim_{\max}$ is more clear in practice and easy to implement. The inductance and capacitance values were chosen to have approx. ½ duty cycle in the light regime

(with a light load: figure 28) at 10 kHz switching frequency and boundary limit range $Lim_{\max} \in \left(\frac{m}{2} + 5, \frac{m}{2} + 10 \right)$.

For the nominal regime results a duty cycle smaller than ½ , that determine a inductor current ripple smaller than imposed value (see [1]). For simulation examples the nominal input voltage, output voltage and output power are $V_{in} = 48V$, $V_{out} = 60V$ and $P_{out} = 900W$, respectively, the work switching frequency is 10 kHz (for the nominal regime). The average inductor current <iL>= IL is $I_L = \frac{I_{out}}{1-\tau} = 18{,}75A$.

For all presented hysteretic controller simulation without clock we choose $I_{L\min}$ =17.75A and $I_{L\max}$ =19.75A, and for all presented hysteretic controller simulation with clock we choose $I_{L\max}$ =21.75A. Also V_{offset}=5·6·1,75V=52,5V, $V_{knee} = 5 \cdot 6 \cdot 2.13V \cong 64\,\text{V}$, V_{max}=5·6·2,45V=73,5V, series resistance of the inductor R_L = 0,05Ω and the calculated equivalent series resistance of the batteries pack is *RS*=5·80 mΩ=0,4 Ω.

(C)BHC, (C)BCCT and (C)HFC were tested in different conditions of usage. In this work are presented the obtained results for the following case:

DC-DC boost converter without energy storage device:

A1. Nominal load ($R_{load} = 4\Omega$): figures 9(a,b), 10(a,b) and 11(a,b), respectively;

All figures have the same composition: on top – phase state trajectory; on middle – inductor current (output voltage) in time; on bottom – q1 switch state (q2 diode state) in time.

A2. Step nominal/light load ($R_{load} = 4\Omega$, respective $R_{load} = 20\Omega$ at 3000μs time after the start): figures 12(a,b), 13(a,b) and 14(a,b), respectively;

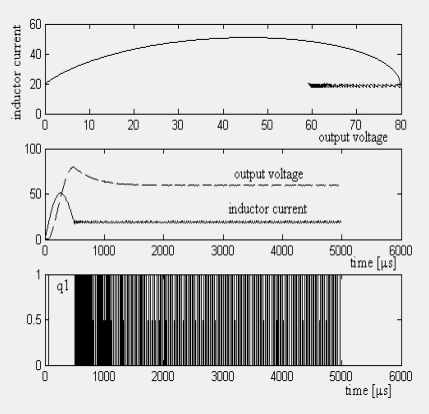

Fig. 9.a - BHC : Nominal load

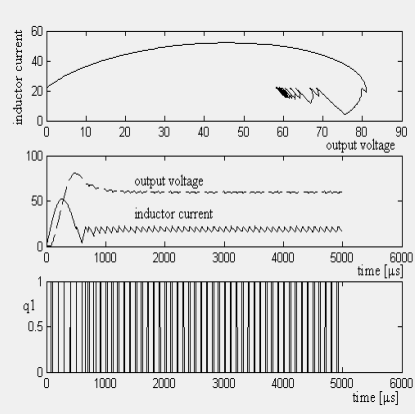

Fig. 9.b - CBHC : Nominal load

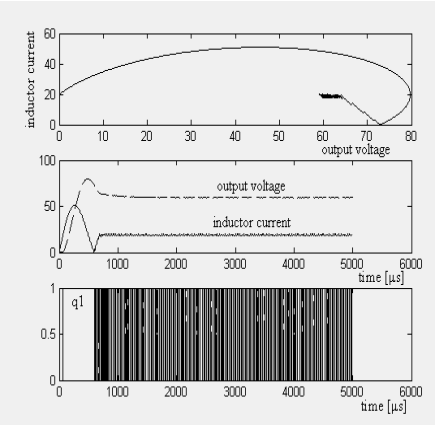

Fig. 10.a - BCCT : Nominal load

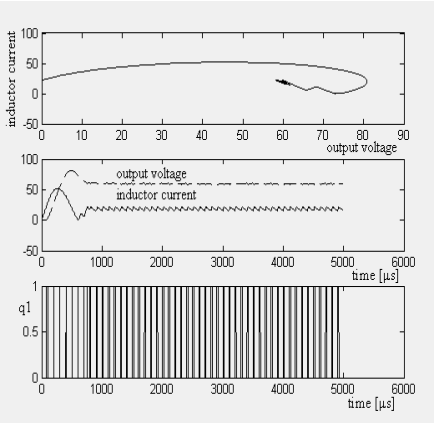

Fig. 10.b - CBCCT : Nominal load

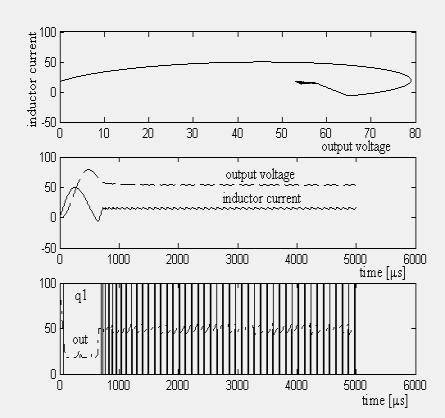

Fig. 11.a - HFC : Nominal load

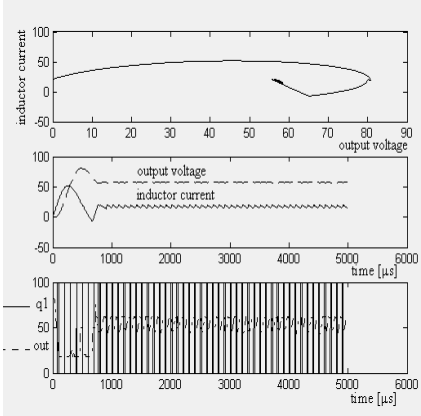

Fig. 11.b - CHFC : Nominal load

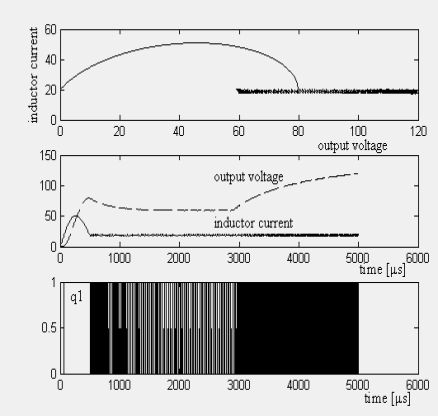

Fig. 12.a - BHC : Step nominal/light load

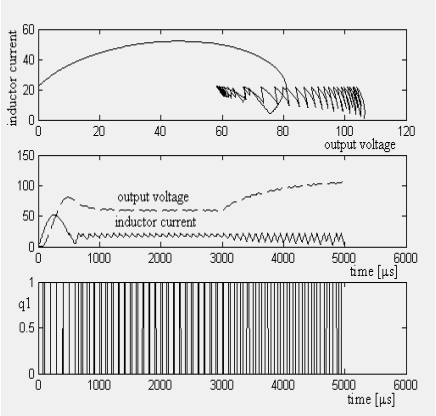

Fig. 12.b - CBHC : Step nominal/light load

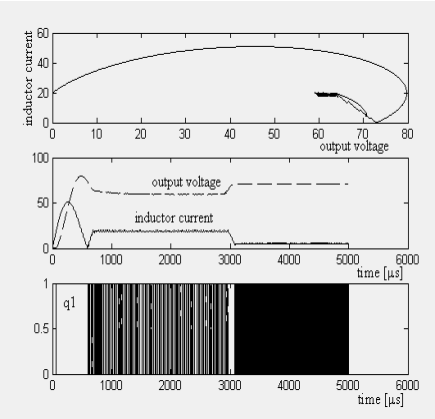

Fig. 13.a - BCCT : Step nominal/light load

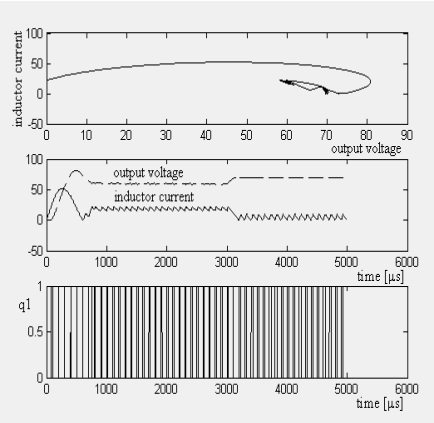

Fig. 13.b - CBCCT : Step nominal/light load

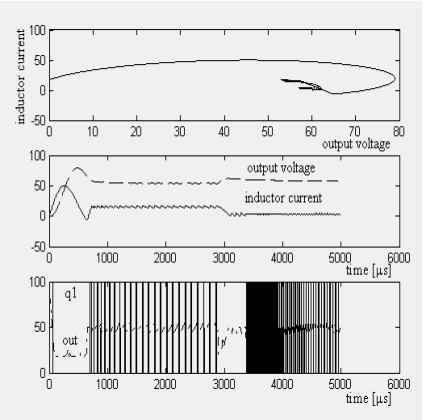

Fig. 14.a - HFC : Step nominal/light load

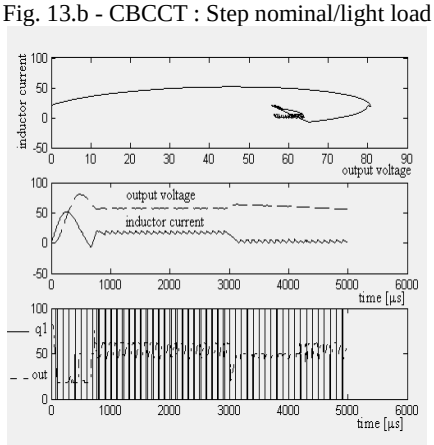

Fig. 14.b - CHFC : Step nominal/light load

To compare the inductor current ripple a zoom of the inductor current is made in nominal steady state regime (figures 12(c,d), 13(c,d) and 14(c,d), respectively).

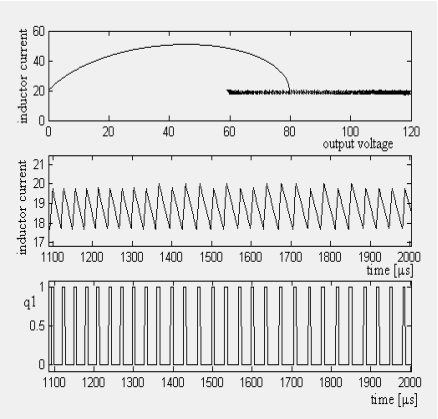

Fig. 12.c - BHC : Step nominal/light load

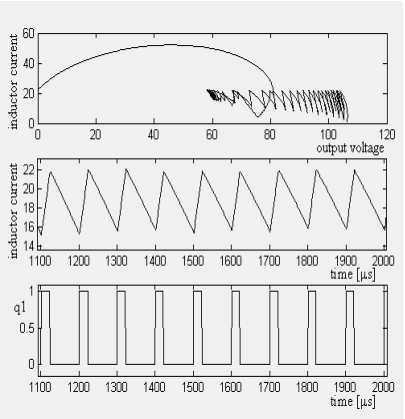

Fig. 12.d - CBHC : Step nominal/light load

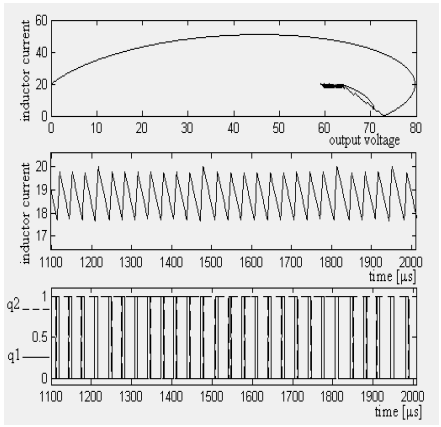

Fig. 13.c - BCCT : Step nominal/light load

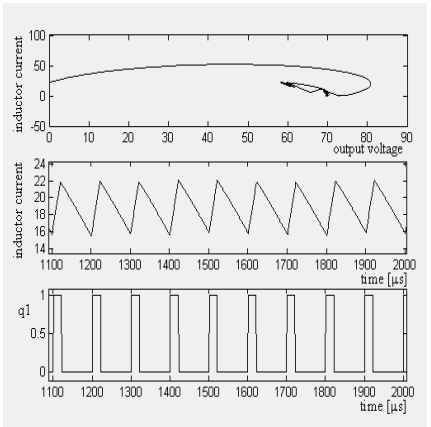

Fig. 13.d - CBCCT : Step nominal/light load

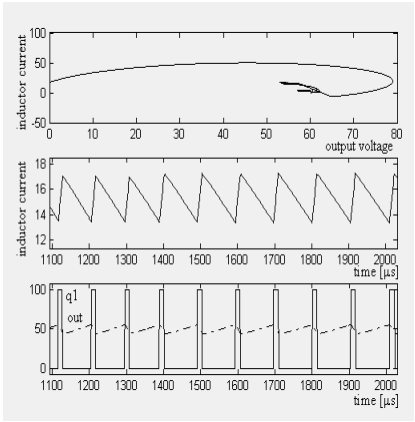

Fig. 14.c - HFC : Step nominal/light load

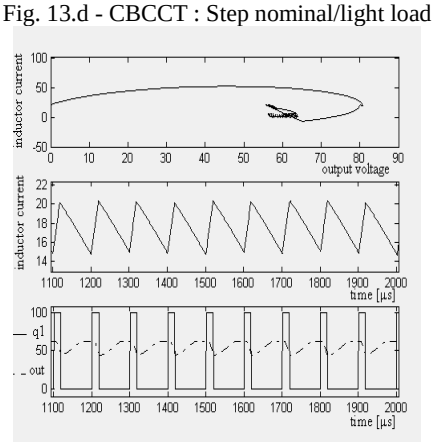

Fig. 14.d - CHFC : Step nominal/light load

A3. Step high/light load ($R_{load} = 2\Omega$, respective $R_{load} = 10\Omega$ at 3000μs time after the start): figures 15(a,b), 16(a,b) and 17(a,b), respectively;

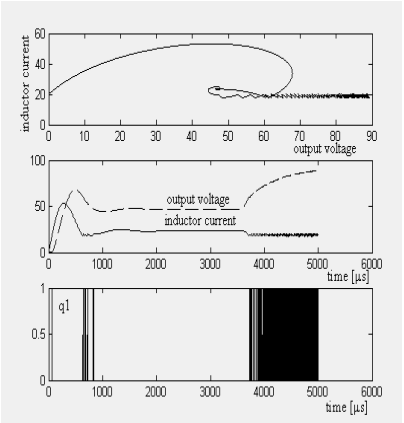

Fig. 15.a - BHC : Step high/light load

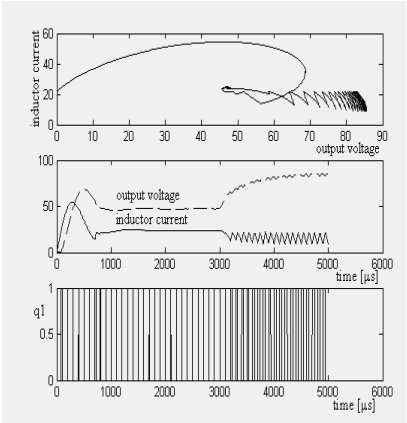

Fig. 15.b - CBHC : Step high/light load

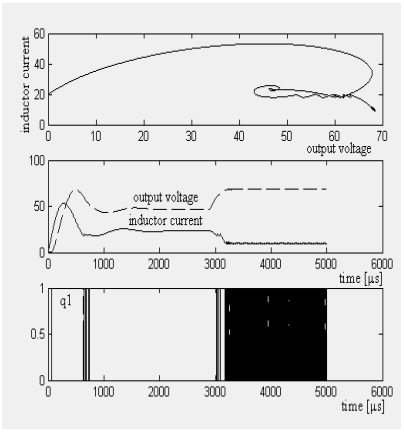

Fig. 16.a - BCCT : Step high/light load

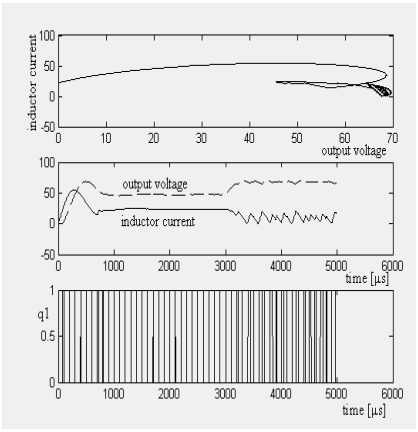

Fig. 16.b - CBCCT : Step high/light load

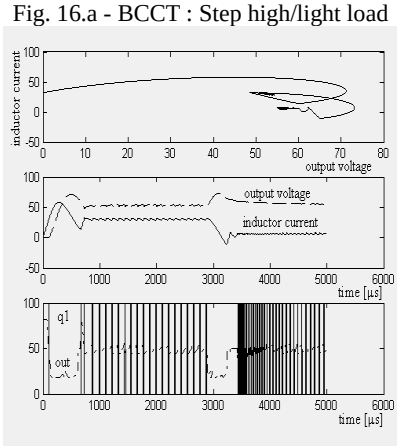

Fig. 17.a - HFC : Step high/light load

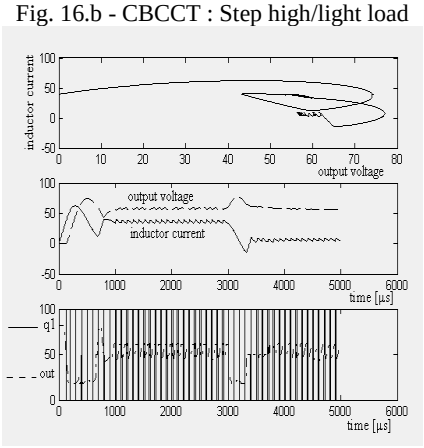

Fig. 17.b - CHFC : Step high/light load

DC-DC boost converter with energy storage device (ESD):

B1. Nominal load ($R_{load} = 4\Omega$); figures 18(a,b), 19(a,b) and 20(a,b), respectively;

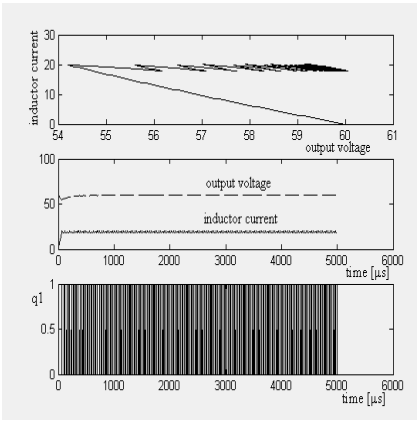

Fig. 18.a - BHC with ESD : Nominal load

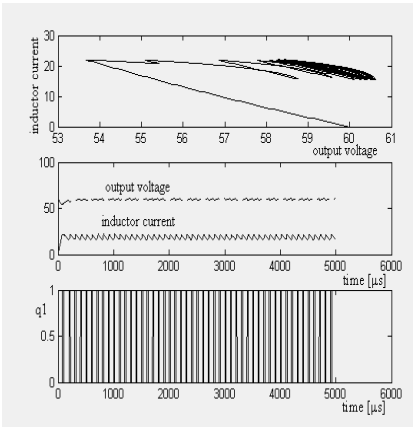

Fig. 18.b - CBHC with ESD : Nominal load

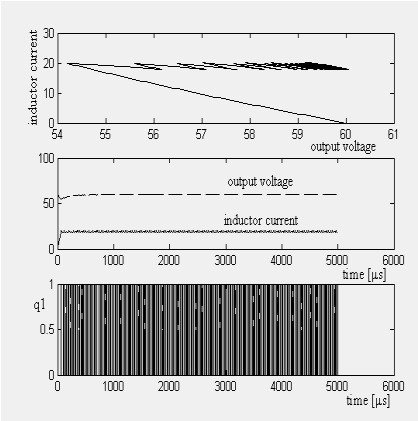

Fig. 19.a - BCCT with ESD : Nominal load

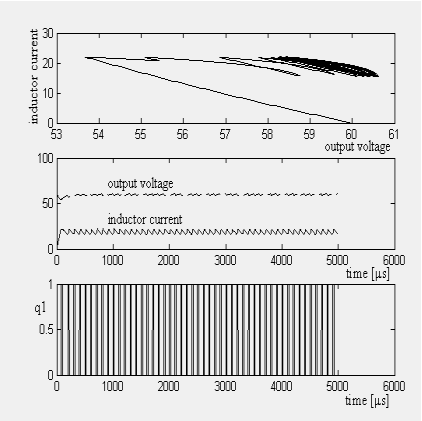

Fig. 19.b - CBCCT with ESD : Nominal load

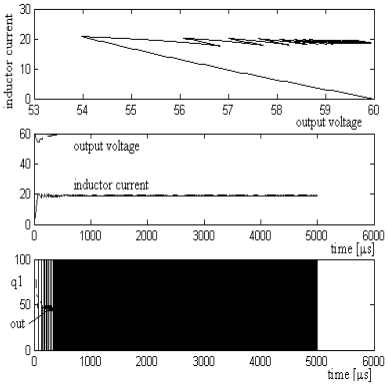

Fig. 20.a - HFC with ESD : Nominal load

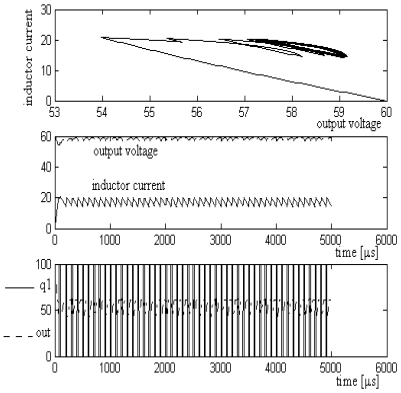

Fig. 20.b - CHFC with ESD : Nominal load

B2. Step nominal/light load ($R_{load} = 4\Omega$, respective $R_{load} = 20\Omega$ at 3000μs time after the start); figures 21a,b), 22(a,b) and 23(a,b), respectively.

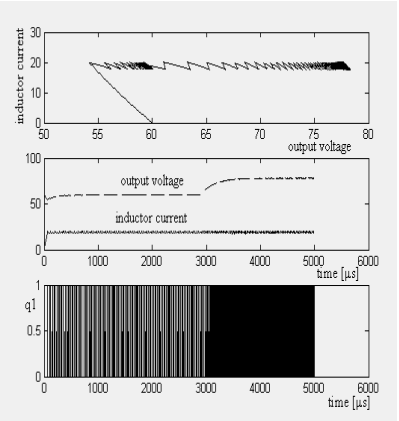

Fig. 21.a - BHC with ESD :
Step nominal/light load

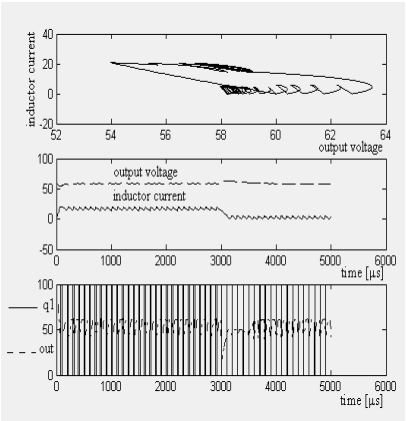

Fig. 21.b - CBHC with ESD :
Step nominal/light load

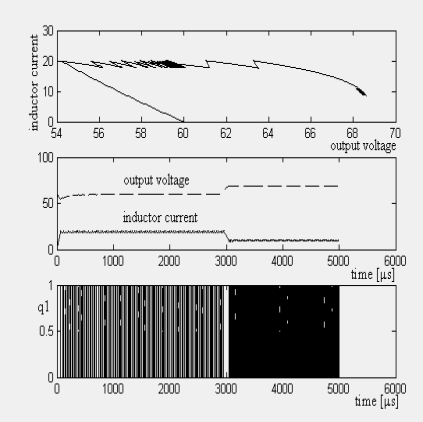

Fig. 22.a - BCCT with ESD:
Step nominal/light load

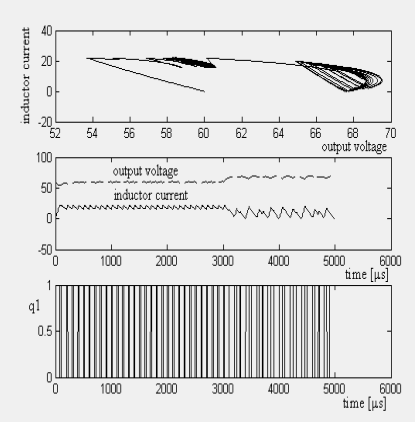

Fig. 22.b - CBCCT with ESD:
Step nominal/light load

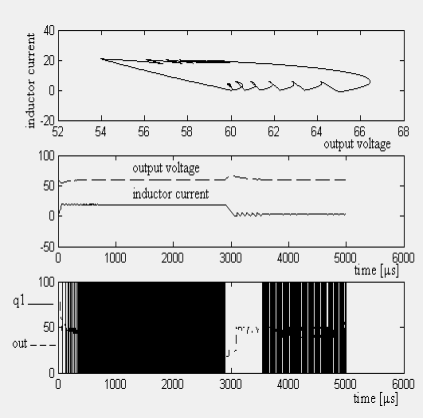

Fig. 23.a - HFC with ESD :
Step nominal/light load

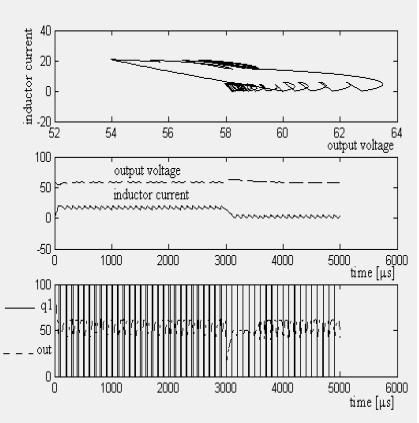

Fig. 23.b - CHFC with ESD :
Step nominal/light load

B3. Step high/light load ($R_{load} = 2\Omega$, respective $R_{load} = 10\Omega$ at 3000μs time after the start); figures 24(a,b), 25(a,b) and 26(a,b), respectively.

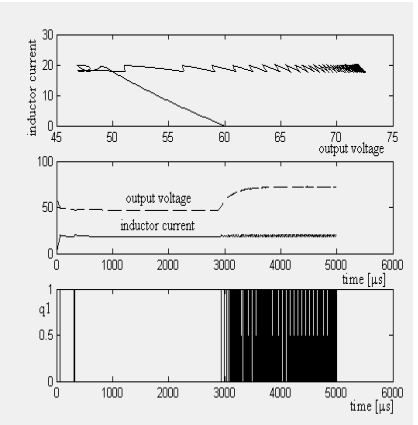

Fig. 24.a-BHC with ESD: Step high/light load

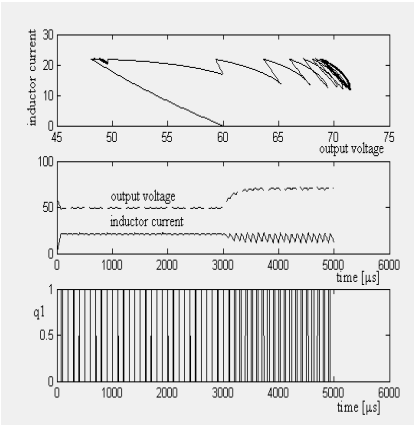

Fig. 24.b-CBHC with ESD: Step high/light load

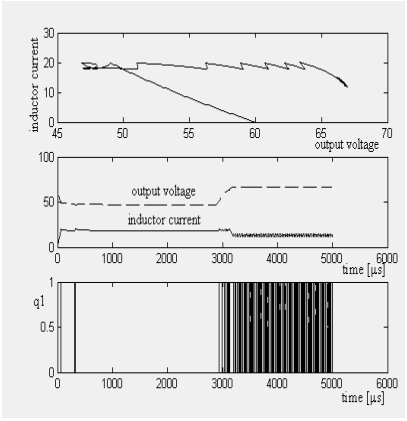

Fig. 25.a-BCCT with ESD:Step high/light load

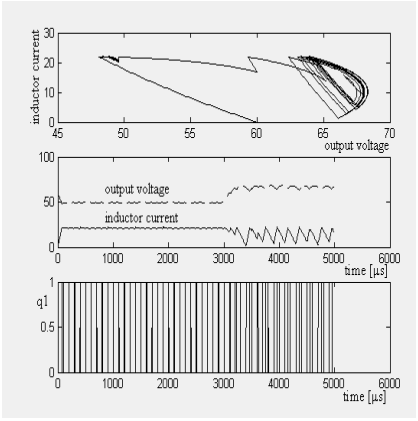

Fig. 25.b-CBCCT with ESD:Step high/light load

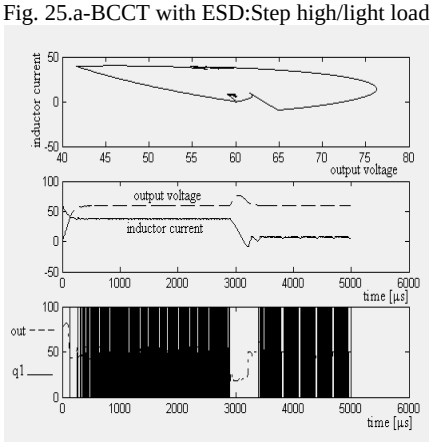

Fig. 26.a - HFC with ESD : Step high/light load

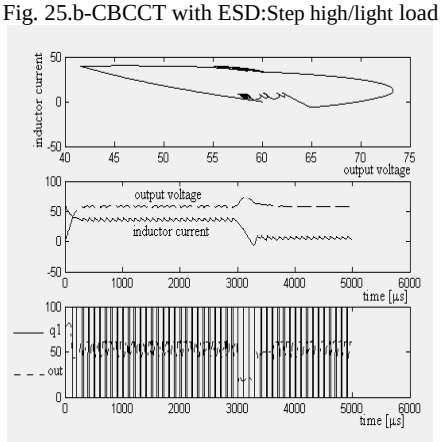

Fig. 26.b - CHFC with ESD : Step high/light load

The inductor current ripple for HFC implementation (figure 27) remain at the same approximate value obtained in nominal steady state regime (figure 11(a,b)).

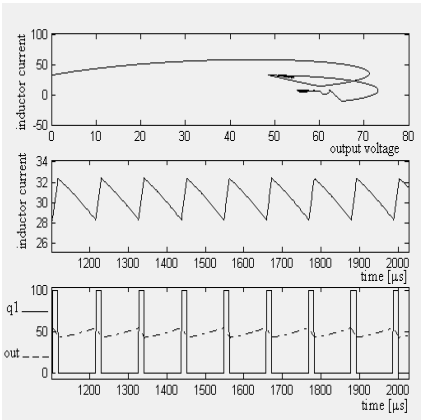

Fig. 27 -. HFC - Step high/light load: zoom

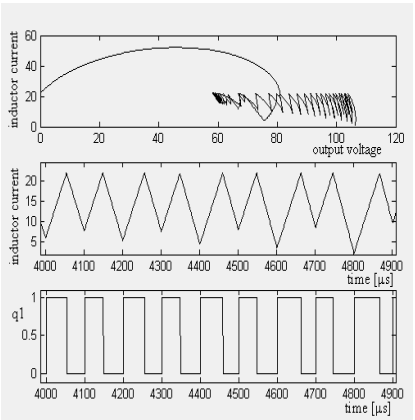

Figure 28. CBHC - Step load: light load zoom

5 CONCLUSION

For a nominal regime with or without energy storage battery the dynamic of the variables is almost the same for different control implementations presented in this paper (CBHC, CBCCT and CHFC). For light load the CBHC implementation can't limit the output voltage of the boost converter because the boost converter works in discontinuous current mode (DCM). An alternative solution which can solve this problem using a BCCT control law is the CBCCT implementation. The complexity of the BCCT controller increases and sometimes it isn't very robust (see figure 13 and figure 19). The performances will rise if the BCCT control law will be a function that depends by the mean inductor current, but this make the BCCT controller more complicate.

The clocked HFC - (C)HFC - implementation (the results presented in this work and other results) permits the emphasizing of the following aspects:

- Clocked HFC improves the energy conversion efficiency of the power converter, indifferently what DC-DC converter topology it is used; this appreciation is indirect sustained by the CFHC control methodology: with fixed switching frequency.
- (C)HFC is a robust controller to parametrical perturbations (for example the design error to boost converter: L, C etc.) ;
- (C)HFC maintains the stationary inductor current ripple in the admitted limits even the large dynamic loads are used (see figures 11,14,17,20 and 23);
- (C)HFC controller can be used for a robust and efficient control of the power converter witch works that an interface between energy source an energy storage device;
- CHFC controller assures less stress on the switching components (MOS transistor and diode) and faster settling after a transient condition (see figures 11,14,17,20 and 23 - b variant comparative with a variant, respectively).

The advantages of (C)HFC control technique include also

- Inherent load-current limiting
- Easy loop-stability design
- No sub-harmonic oscillation
- Instantaneous response to load-current changes
- Constant peak-to-average inductor-current ratio.

At the first look, the output voltage ripple should be defined by the hysteresis at the 'hysteretic comparator' only.

As mentioned, there are some disadvantages for hysteretic control structure without clock. As the switching frequency is not set by a controlled oscillator, it will vary with different external components and with input voltage changes. If the switching frequency has to be fixed in a certain application it might be difficult to find the right design. The principal factors that define the switching frequency are the input voltage, the inductivity value of the inductor and the equivalent serial resistance (ESR) of the output capacitor. As many capacitors change their ESR

over temperature, the switching frequency will change as well. A good trick is to fix the ESR of the output capacitor by using a ceramic capacitor that has a very low maximum ESR (over-temperature and frequency) of about 10 mΩ.

The obtained results are very promising, validating the model of the proposed hysteretic fuzzy control.

References

[1] N. BIZON, *Power converters* (in Romanian), Ed. MatrixROM, Bucharest, 2004.

[2] J. P. AGRAWAL, *Power electronic systems: theory and design*, Upper Saddle River, N.J.: Prentice Hall, 2001.

[3] I. BATARSEH, *Power electronic circuits*, Hoboken, NJ: John Wiley, 2004.

[4] H.J. BERGVELD, (editor), S. J. WANDA S. KRUIJT, P. H. L. NOTTEN, *Battery management systems: design by modeling*, Dordrecht; Boston: Kluwer Academic, 2002.

[5] R. BAUSIERE, F. LABRIQUE, G. SEGUIER, *Power Electronic Converters : DC-DC Conversion*, Berlin; New York: Springer-Verlag, 1992

[6] K. GANSKY, *Rechargeable Batteries Applications Handbook*, Butterworth Heinemann, 1992.

[7] R. W. ERICKSON and D. MAKSIMOVIC, Kluwer Academic Publishers, 2000.

[8] N. BIZON, *Power Electronics Devices* (in Romanian), Ed. MatrixROM, Bucharest, 2002.

[9] N. NED, *Advanced Electric Drives: Analysis, Control and Modeling using Simulink*, MNPERE, 2001.

[10] N. BIZON, *Systems Theory and applications* (in romanian), Ed. MatrixROM, Bucharest, 2004.

[11] T. R. CROMPTON, *Battery Reference Book*, 2nd ed., Butterworth Heinemann, Mass., 1995.

[12] T. A. FROESCHLE, *Current-Mode Controlled Two-State Modulation*, US Patent #4,456,872, January 26, 1984.

[13] C.K. TSE, Y.M. LAI AND H.H.C. IU, *Hopf Bifurcation and Chaos in a Hysteretic Current-Controlled Cuk Regulator*, IEEE Power Electronics Specialists Conference, (PESC'98), Fukuoka Japan, pp. 1091-1097, May 1998.

[14] J. ABU-QAHOUQ, N. PONGRATANANUKUL, I. BATARSEH and T. KASPARIS, *Multiphase Voltage-Mode Hysteretic Controlled VRM with DSP Control and Novel Current Sharing*, IEEE Fourth International Caracas Conference on Devices, Circuits and Systems, P017-1 -P017-7, Aruba, April 17-19, 2002.

[15] S.C. TAN, Y.M. LAI, C.K. TSE and M.K.H. CHEUNG, *An Adaptive Sliding Mode Controller for Buck Converter in Continuuous Conduction Mode*, *IEEE* Applied Power Electronics Conference and Exposition, (APEC'04), pp. 1395-1400, February 2004.

[16] C.K. TSE, W.C.Y. CHAN, *Instability and Chaos in a Current-Mode Controlled Cuk Converter*, IEEE Power Electronics Specialists Conference, (PESC'95), pp. 608-613, Atlanta USA, June 1995.

[17] L. A. ZADEH: *Fuzzy Sets*, Information and Control, vol.8, pp.338-353, 1965.

[18] E. SOFRON, N. BIZON, S. IONITA, R. RADUCU, *Fuzzy control systems – modeling and designing* (in Romanian), Ed. All, Bucharest, 1999.

[19] W.C. SO, C.K. TSE and Y.S. LEE, *Development of a Fuzzy Logic Controller for DC/DC Converters: Design, Computer Simulation and Experimental Evaluation*, IEEE Transactions on Power Electronics, vol. 11, no. 1, pp. 24-32, January 1996.